UMYU Scientifica, Vol. 4 NO. 1, March 2025, Pp 374 – 378
https://doi.org/10.56919/usci.2541.037
ISSN: 2955 – 1145 (print); 2955 – 1153 (online)
A periodical of the Faculty of Natural and Applied Sciences, UMYU, Katsina

ORIGINAL RESEARCH ARTICLE

Phase transformation and thermal stability studies of Fe-doped ZnSe nanocrystals

Ibrahim Muhammad Bagudo[1]*, Abdullahi Tanimu[1] and Aminu Y. Sabiru[1]
[1]Department of Physics, Umaru Musa Yar'adua University Katsina, Nigeria

ARTICLE HISTORY
Received December 23, 2024
Accepted March 28, 2025
Published March 31, 2025

KEYWORDS
Mechanochemical synthesis, nanocrystal, doping process, thermal property, phase transformation

ABSTRACT
This study explored the phase transformation in ZnSe doped with Fe ions via XRD, TGA, and HRTEM analyses. The X-ray diffraction pattern of the Fe-doped ZnSe nanocrystal milled for 5 hours, 10 hours, and 20 hours revealed a cubic phase structure that became progressively stable after 5 hours of milling. The XRD peaks broadened with increasing milling time, suggesting a decrease in the crystallite size of 4.2 nm after 20 h of milling, as evaluated by Scherre's formula. High-resolution transmission electron microscopy (HR-TEM) revealed well-defined lattice fringes with an interplanar spacing of approximately 0.38 nm. The thermal properties of the milled powder were characterized via differential scanning calorimetry (DSC) and thermogravimetric analysis (TGA). The endothermic peak increases linearly from 230–475 °C, whereas the exothermic peak decreases and later increases with increasing milling time. The thermal stability of the Fe-doped ZnSe nanocrystal improved as the milling progressed, and a weight loss of 14–4% was recorded.

INTRODUCTION
Dilute magnetic semiconductor quantum dots (DMSQDs) are nonmagnetic quantum dots that are doped with paramagnetic ions. This class of material has received considerable attention from researchers (Dutta et al., 2022; Kobak et al., 2014; Yadav et al., 2020). The magneto-optic properties of these materials arise from magnetic exchange interactions between the transition metal dopants and the host nonmagnetic material, which offers unique opportunities for diverse applications. The electronic material formed can support spin transport at or above room temperature. Their potential applications, such as in spin field transistors, spin-emitting diodes, spin-resonator devices, and quantum bits for quantum computation, are few among the motivation factors for their study.

Recently, interest in iron-doped II-VI semiconductors as potential materials in the field of spintronics has increased. The material has some distinctive optical and spin glass magnetic behaviors. Notably, this material's magnetic coupling onset depends on carriers and iron aggregation in the host (Bindra et al., 2018; Twardowski et al., 1985). The ability of Fe(III) to form clusters in nonmagnetic materials has been observed in many systems that eventually give rise to spin frustration comparable to that found in Kagome lattice structures(Kurian & Mochena, 2020). Magnetic interactions are frustrated if a spin cannot arrange its orientation in such a way that it can benefit from exchange interactions with its neighboring spins. Moreover, for a high-performance electronic device, understanding the material's thermal stability and phase transition is vital. Furthermore, the optical and electrical properties of ZnSe can be tuned for a specific application by simply introducing transition metal ions into the energy band gap, which in turn produces deep levels.

For example, in a solar cell device, the low thermal stability of planar perovskites is associated with the occurrence of a phase transition between tetragonal and cubic structures, which stirs up phase transition-induced carrier traps. This subsequently promotes rapid device degradation through changes in the crystalline lattice due to defect formation around the grain boundaries(Qin et al., 2019).

Notably, phase transformation and thermal stability are fundamental for understanding a material's physical and chemical properties. Hence, it is important to explore the fundamental physics involved in the phase transition at the nanoscale for effective applications(Li & Yang, 2010).

Several researchers have reported exchange interactions in iron-doped ZnSe [(Bindra et al., 2018),(de Moraes et al., 2002),(Swagten et al., 1989)], but reports on the thermal stability and phase transformation of bulk materials are limited. (Marangolo et al., 2002) reported that the thermal stability of the Fe/ZnSe (001) interface lattice remains at 360 °C during the annealing process. For a (100)-oriented single-crystalline Fe/ZnSe interface, the thermal stability persists up to 450 °C, whereas polycrystalline Fe/ZnSe

Correspondence: Ibrahim Muhammad Bagudo. Department of Physics, Faculty of Natural and Applied Sciences, Umaru Musa Yar'adua University Katsina, Nigeria. ✉ ibrahim.bagudo@umyu.edu.ng.
How to cite: Muhammad, I. B., Tanimu, A., & Sabiru, A. Y. (2025). Phase transformation and thermal stability studies of Fe-doped ZnSe nanocrystals. *UMYU Scientifica*, 4(1), 374 – 378. https://doi.org/10.56919/usci.2541.037

suffers fast diffusion at the growth temperature (Sou et al., 2005). To the best of our knowledge, there are no reports at the nanoscale on the thermal stability and phase transformation of this material synthesized via a mechanochemical route.

Among the other experimental tools, TGA provides information on a material's thermal stability and decomposition by measuring the change in mass as a function of temperature or time. In addition, DSC determines the energy absorbed or released by a material during phase transitions such as crystallization or melting. Material phase transformation and thermal stability properties are of high interest because of their importance in determining device performance (Fatahi et al., 2022; Müller et al., 2020; Sekerci & Yakuphanoglu, 2004).

In this work, we report the synthesis of Fe-doped ZnSe quantum dots through a high-energy ball milling process. The structure, morphology, phase transformation, and thermal stability were studied via X-ray diffraction (XRD), high-resolution transmission electron spectroscopy (HRTEM), DSC, and TGA.

MATERIALS AND METHODS

High-purity iron (III) (99.99%), zinc (99.99%), and selenium (99.99%) elemental powders were purchased from Alfa Aesar. The combinations of the three elements were thoroughly mixed at the desired atomic ratios before being placed in the grinding jar. The mixture was subsequently transferred and vacuum-packed in a stainless-steel grinding jar containing stainless steel balls under an inert atmosphere. A high-energy planetary ball mill PM 100 (Retsch) with a ball-to-powder ratio of 10:1 was used. Grinding balls 3 mm in diameter were used. The milling time was varied from 5--20 hours at a speed of 300 rpm (rpm). The first sample was collected after 5 hours of milling. A small quantity of the as-milled powder was further collected from the grinding jar for 10 and 20 hours. The samples were analyzed for microstructural and thermal stability.

The microstructural characterization was performed via a PANalytical X'PertPRO X-ray diffractometer with Cu Kα radiation [λ=1.54056Å]. The XRD sample holder was filled with 5 grams of milled powder and then transferred to the sample compartment of the XRD machine. The diffractograms were recorded in the range of 2 theta (20--90^0) with a step size of 0.8 s. The alloying mechanism of the milled powder with increasing milling was observed by monitoring the changes in the XRD diffraction peaks. Each powder sample's surface morphology and composition were analyzed via field-emission scanning electron microscopy via a Nova Nano SEM 230**.** High-resolution transmission electron microscopy (HRTEM) at 200 kV with field emission (Tecnai G2 20 S-TWIN, FEI) was used to monitor the structural evolution of the milled powders. We dissolved 10 mg of the milled samples in ethanol solution, sonicated them for 15 minutes and later drop cast them on a grid placed on the surface of a piece of tissue paper. The grid was dried under a vacuum for 30 minutes and finally placed in the sample chamber of the HRTEM instrument. The image of the 20-hour milled sample was recorded under (10^6) magnification. The thermal stability was determined. DSC/TGA (Brand: Mettler Toledo, Model: TGA/DSC1. The samples were made into compacted pellet discs by pressing 3 g of the milled powder under 50 kN force. The pellet was placed into the sample compartment for DSC/TGA analyses at different heating rates.

RESULTS AND DISCUSSION

A. XRD characterization

The X-ray diffraction patterns of the powders milled for 5 h, 10 h, and 20 h at different milling times are presented in Figure 1(a-c). All diffraction peaks are indexed to the (111), (002), (022), (113), (004), and (133) lattice planes in the cubic phase structure (space group F-4 3 m), which correspond to the ICSD (98-008-1168) and ICD (98-009-2286) planes.

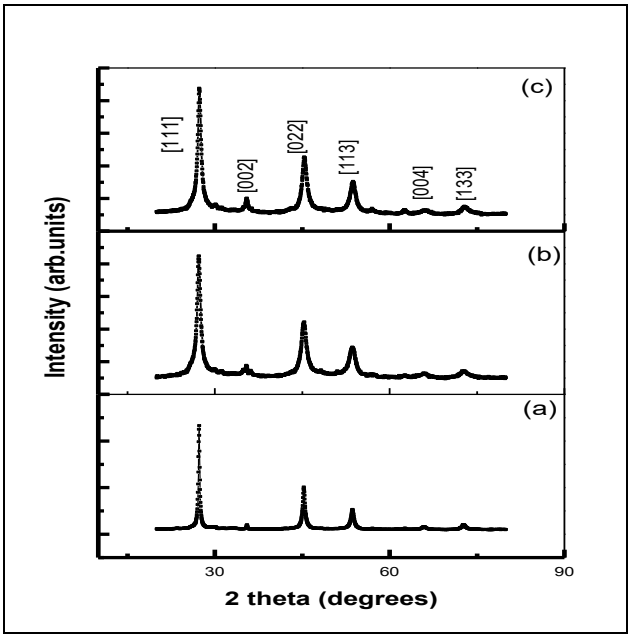

Figure 1. XRD patterns of (a) 5 h, (b) 10 h, and (c) 20 h milled Fe-doped ZnSe

The diffraction peaks became broader with increasing milling time, whereas their intensities decreased. The broad nature of the diffraction peaks could be interpreted in two ways. One possible explanation is the refinement of the crystallite size accompanied by internal stress induced by the milling process. The second peak might indicate iron substitutions into the ZnSe lattice host (Saikia et al., 2016). A weak diffraction peak (002) at approximately d= 2.5 became prominent after 10 h of milling. The intensity of this peak increases with increasing milling time, which is attributed to the evolution of the stable phase [2]. The crystallite size was calculated via the Scherrer formula

$$D = \frac{0.9 \times \lambda}{\beta \cos \theta_B} \quad (1)$$

D is the crystallite size, λ is the X-ray wavelength (1.5405 Å), β is the full width at half maximum, and θ_B is the Bragg angle.

B. Surface morphology

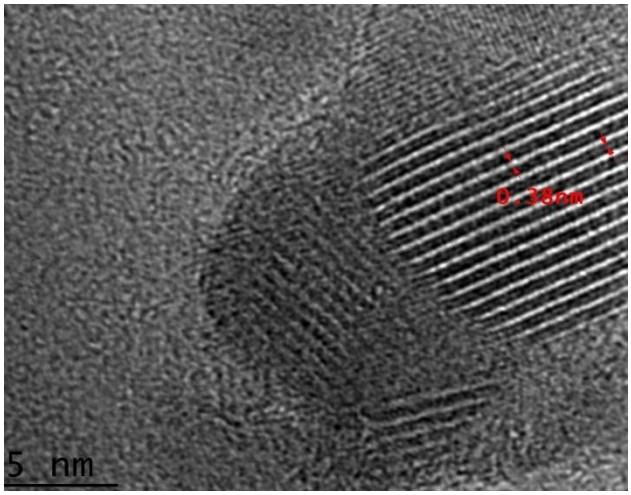

Figure 2. HRTEM image of the Fe-doped ZnSe sample after 20 h

To gain insight into the crystallinity of the Fe-doped ZnSe nanocrystal, a high-resolution transmission electron microscopy (HRTEM) image of the 20 h milled sample is presented in Fig. 2. The lattice fringes have a well-defined interplanar spacing of approximately 0.38 nm, which is in good agreement with 0.32 nm. The regular fringes observed imply good crystallinity with limited structural defects in the milled powder after 20 h of milling.

C. Thermal analysis and phase transformation

To study the thermal stability of the milled powders, we performed TG and DSC measurements on the milled samples.

Figure 3 shows DSC thermograms obtained at 10 0C/min heating rates for all three samples. A careful examination of the DSC curve indicates the existence of three thermal anomalies. Interestingly, two endothermic peaks (D2&D3) were observed within the 230–475 °C temperature range. Similarly, an exothermic peak (D1) corresponds to 771 ^{0}C, 754 ^{0}C, and 775 ^{0}C for the samples milled for 5 h, 15 h, and 20 h, respectively. The endothermic peaks could be associated with melting the c-Se phase in the parent compound (Hou et al., 2013). The selenium crystallization temperature is approximately 150 °C, whereas the melting temperature of the parent compound of ZnSe is 210 °C. The broad exothermal peak is attributed to the phase transition from the zinc blend structure to the wurtzite structure upon continuous milling.

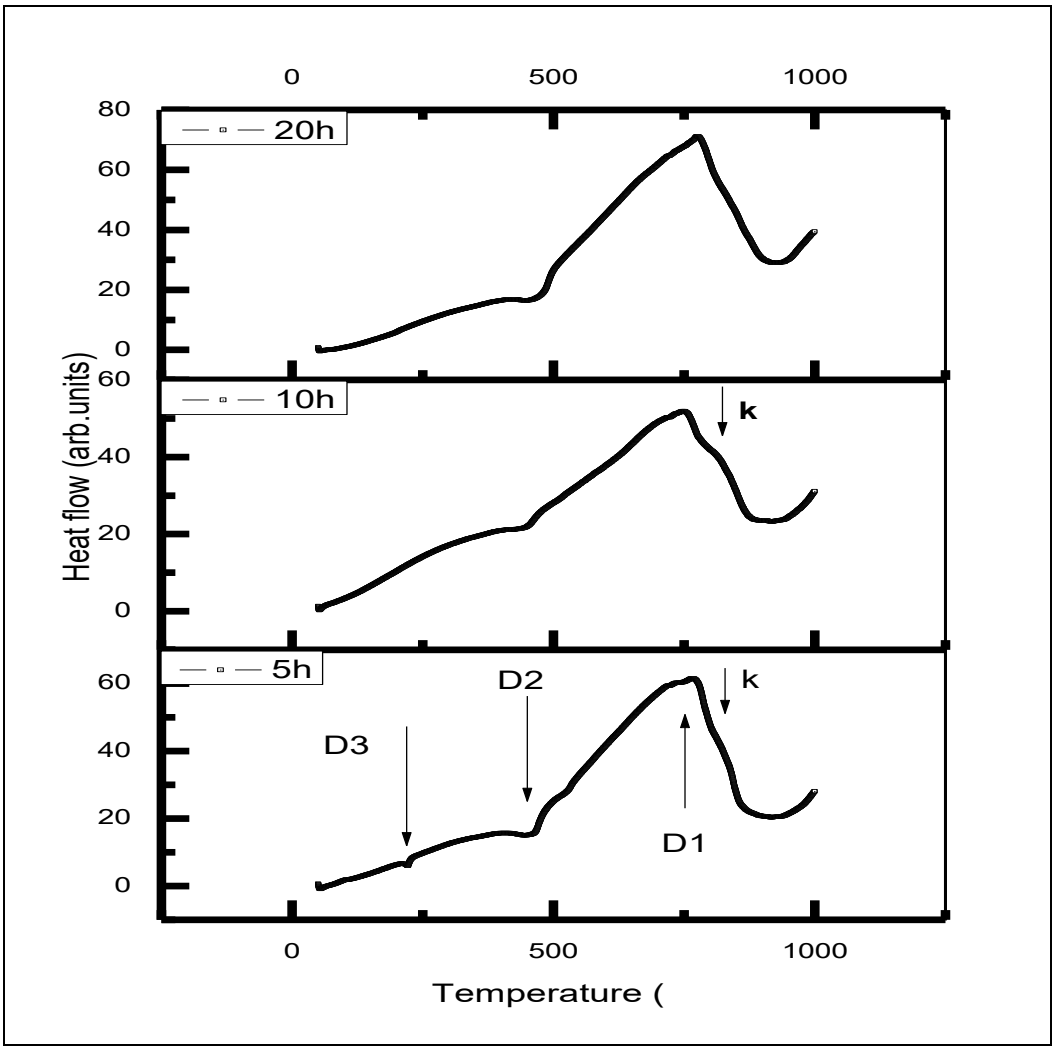

Figure 3. DSC thermogram of the Fe-doped ZnSe nanocrystal

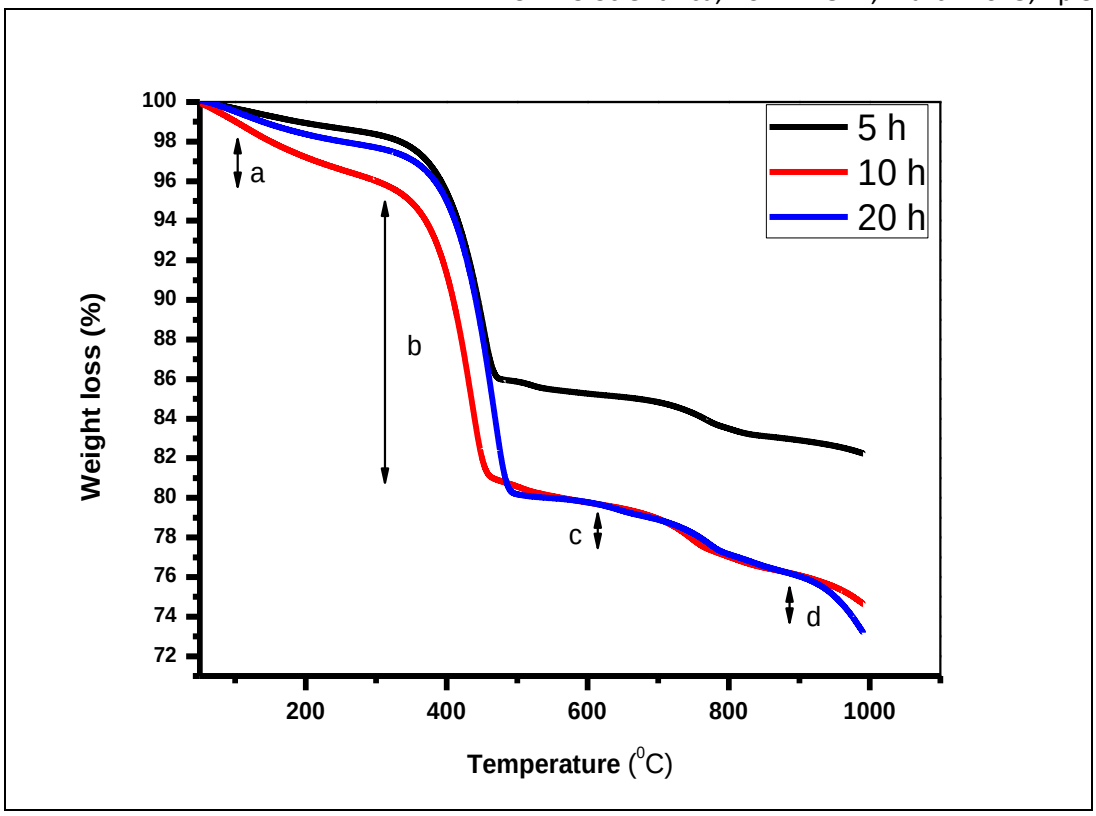

Figure 4. TGA curves of the Fe-doped ZnSe nanocrystals

Fig. 4 shows the TGA curves resulting from the thermal decomposition of the samples. The thermal decomposition corresponds to 10%, 14%, and 4% weight loss of the 5 h, 10 h and 20 h milled samples, respectively. The thermal stability observed in the 20 h milled sample might be due to the diffusion of Fe into a solid solution of the CdSe structure, forming a final stable phase. This can be corroborated by the increasing intensity of the (002) plane. The decomposition curve is divided into four regions (a, b, c, and d), which is inferred to indicate that at least four phase transformation stages occurred during the milling process before a stable phase of the FeZnSe nanocrystals was obtained. We note that lower decomposition might not necessarily translate to higher stability; for such assessments, other factors must be considered (Burwig et al., 2022). This will be our topic for the next paper.

$$K(T) = A \exp(-E/RT) \quad (2)$$

where R is the universal gas constant, E is the activation energy, and A is the preexponential factor.

CONCLUSIONS

In summary, we investigated the structural and thermal stability of iron-doped ZnSe nanocrystals via a mechanochemical route. Our results revealed that the diffraction peaks became broader with increasing milling time, whereas the peak intensities decreased. Crystalline fringes with interplanar spacing from the morphology of 20 h milled samples. Compared with the other samples, the 20 h milled sample exhibited a slow decomposition rate, with only a 4% weight loss. The evolution of the (001) diffraction peaks and small weight loss could be attributed to the stable phase of the Fe-doped ZnSe nanocrystals.

CONFLICT OF INTEREST

The authors declare no conflicts of interest.

ACKNOWLEDGMENT

The authors gratefully acknowledge the financial support of the tertiary education trust fund (TETFund) Nigeria. The grant is provided under the TETFund institution-based research intervention allocation

REFERENCES

Bindra, J. K., Gutsev, L. G., Van Tol, J., Singh, K., Dalal, N. S., & Strouse, G. F. (2018). Experimental validation of ferromagnetic-antiferromagnetic competition in FexZn1−xSe quantum dots by computational modeling. *Chemistry of Materials, 30*(6), 2093–2101. **[Crossref]**

Burwig, T., Heinze, K., & Pistor, P. (2022). Thermal decomposition kinetics of $FAPbI_3$ thin films. *Physical Review Materials, 6*(6), 1–12. **[Crossref]**

de Moraes, A. R., Silveira, E., Mosca, D. H., Mattoso, N., & Schreiner, W. H. (2002). Surface-enhanced Raman scattering for magnetic semiconductor ZnSe:Fe hybrid structures. *Physical Review B - Condensed Matter and Materials Physics, 65*(17), 1724181–1724184. **[Crossref]**

Dutta, A., Almutairi, A. S., Joseph, J. P., Baev, A., Petrou, A., Zeng, H., & Prasad, P. N. (2022). Exploring magneto-optic properties of colloidal two-dimensional copper-doped CdSe nanoplatelets. *Nanophotonics, 11*(22), 5143–5152. **[Crossref]**

Fatahi, H., Claverie, J., & Poncet, S. (2022). Thermal characterization of phase change materials by differential scanning calorimetry: A review. *Applied Sciences, 12*(23), 12019. **[Crossref]**

Hou, C., Jia, X., Wei, L., Stolyarov, A. M., Shapira, O., Joannopoulos, J. D., & Fink, Y. (2013). Direct atomic-level observation and chemical analysis of ZnSe synthesized by in situ high-throughput reactive fiber drawing. *Nano Letters, 13*(3), 975–979. **[Crossref]**

Kobak, J., Smoleński, T., Goryca, M., Papaj, M., Gietka, K., Bogucki, A., Koperski, M., Rousset, J.-G., Suffczyński, J., Janik, E., Nawrocki, M., Golnik, A., Kossacki, P., & Pacuski, W. (2014). Designing quantum dots for solotronics. *Nature Communications, 5*(1), 3191. **[Crossref]**

Kurian, G., & Mochena, M. (2020). First principles investigations of Fe^{3+} impurity and Fe^{3+} + $V^{-}Cd$ complex in strongly confined CdSe quantum dot. *Journal of Applied Physics, 128*(17). **[Crossref]**

Li, S., & Yang, G. W. (2010). Phase transition of II−VI semiconductor nanocrystals. *The Journal of Physical Chemistry C, 114*(35), 15054–15060. **[Crossref]**

Marangolo, M., Gustavsson, F., Eddrief, M., Sainctavit, P., Etgens, V. H., Cros, V., Petroff, F., George, J. M., Bencok, P., & Brookes, N. B. (2002). Magnetism of the [Formula presented] interface. *Physical Review Letters, 88*(21), 4. **[Crossref]**

Müller, L., Rubio-Pérez, G., Bach, A., Muñoz-Rujas, N., Aguilar, F., & Worlitschek, J. (2020). Consistent DSC and TGA methodology as basis for the measurement and comparison of thermo-physical properties of phase change materials. *Materials, 13*(20), 4486. **[Crossref]**

Qin, C., Matsushima, T., Klotz, D., Fujihara, T., & Adachi, C. (2019). Device stability: The relation of phase-transition effects and thermal stability of planar perovskite solar cells (Adv. Sci. 1/2019). *Advanced Science, 6*(1), 499–506. **[Crossref]**

Saikia, D., Raland, R., & Borah, J. P. (2016). Influence of Fe doping on the structural, optical and magnetic properties of ZnS diluted magnetic semiconductor. *Physica E: Low-Dimensional Systems and Nanostructures, 83*, 56–63. **[Crossref]**

Sekerci, M., & Yakuphanoglu, F. (2004). Thermal analysis study of some transition metal complexes by TG and DSC methods. *Journal of Thermal Analysis and Calorimetry, 75*(1), 189–195. **[Crossref]**

Sou, I. K., Wang, C., Chan, S. K., & Wong, G. K. L. (2005). Thermal diffusion studies of MBE-grown ZnSe/Fe/ZnSe and ZnS/Fe/ZnS structures. *Journal of Crystal Growth, 278*(1–4), 282–287. **[Crossref]**

Swagten, H. J. M., Twardowski, A., De Jonge, W. J. M., & Demianiuk, M. (1989). Magnetic properties of the diluted magnetic semiconductor $Zn_{1-x}Fe_xSe$. *Physical Review B, 39*(4), 2568–2577. **[Crossref]**

Twardowski, A., Von Ortenberg, M., & Demianiuk, M. (1985). Magnetization of ZnFeSe semimagnetic semiconductors. *Journal of Crystal Growth, 72*(1–2), 401–404. **[Crossref]**

Yadav, A. N., Bindra, J. K., Jakhar, N., & Singh, K. (2020). Switching-on superparamagnetism in diluted magnetic Fe(III) doped CdSe quantum dots. *CrystEngComm, 22*(10), 1738–1745. **[Crossref]**